A Dielectric Loaded Resonator for the Measurement of the Complex Permittivity of Dielectric Substrates

Andrea Alimenti[ID], *Member, IEEE*, Erika Pittella[ID], *Member, IEEE*, Kostiantyn Torokhtii[ID], *Member, IEEE*, Nicola Pompeo[ID], *Senior Member, IEEE*, Emanuele Piuzzi[ID], *Member, IEEE*, and Enrico Silva[ID], *Senior Member, IEEE*

Abstract—A new configuration of dielectric-loaded resonator (DR), particularly versatile for the complex permittivity measurement of substrates for microwave circuits, even in the presence of back metal plates, is shown here. To test this technique in a wide interval of the values of the complex permittivity, the versatility of 3-D printing is exploited to print samples with different densities, thus artificially changing the effective permittivity in the interval (1.7–3.1) for the real part and (0.02–0.06) for the imaginary part. The designed resonator, tuned at ∼12 GHz, is experimentally validated by the comparison of measurements obtained on these samples with a split ring resonator (SRR) and standard transmission/reflection waveguide methods. Then, the versatility of the designed resonator is shown in the characterization of FR4-fiberglass and Kapton polyimide samples.

Index Terms—Complex permittivity measurement, dielectric-loaded resonator (DR), microwave, split ring resonator (SRR).

I. INTRODUCTION

DUE to the importance of accurate knowledge of the high-frequency electromagnetic (e.m.) properties of dielectric materials, in particular, in view of the development of information and communication technologies (ICT), several microwave measurement techniques have been developed since the 1950s to meet the different operative needs in terms of measurement frequencies, geometries, and dimensions of the investigated samples as well as accuracy and sensitivity levels [1], [2], [3]. These measurement methods are traditionally divided into two macrocategories: 1) broadband transmission/reflection methods and 2) resonant. The great advantage of transmission/reflection methods lies in their wide and continuous frequency band of operation. However, their poor sensitivity makes these methods not appropriate for precise and accurate characterizations of low-loss materials [2], [3], [4], [5]. On the contrary, resonant techniques, which operate only at discrete frequencies, take advantage of the high sensitivity of the quality factor Q and resonance

frequency f_0 of electromagnetically resonating structures to small variations in the e.m. properties of the system elements. Depending on the sample e.m. and geometrical properties, different kinds of resonant fixtures can be found in literature [1], [2], for example, cavities, dielectric-loaded resonators (DRs), dielectric resonators, open resonators, and planar resonators.

To achieve the best performances, the fixture choice depends on the characteristics of the sample (size and state of matter), e.m. properties (insulators/conductors), and operating conditions (frequency in the intended application).

In this work, we propose the use of a modified configuration of a DR for the measurement of the dielectric substrates relative complex permittivity $\tilde{\varepsilon}_r = \varepsilon'_r - i\varepsilon''_r$, with $\varepsilon'_r = \text{Re}\,\tilde{\varepsilon}_r$, $\varepsilon''_r = -\text{Im}\,\tilde{\varepsilon}_r$, $i^2 = -1$. The ratio $\tan\delta = \varepsilon''_r/\varepsilon'_r$ is known as the loss tangent. Thanks to their high sensitivity, DRs are widely used both for surface resistance measurement of normal conductors, surface impedance measurement of superconductors, and complex permittivity measurements of low-loss dielectrics [1], [2], [6], [7], [8], [9], [10], [11], [12]. Despite their common use with low-loss materials, in this work we show the possibility of using this measurement fixture also for the characterization of lossy dielectric materials without losing sensitivity. A new closed kind of configuration, which does not require completely unmounting the resonator for sample loading, is exploited. In particular, the presented geometry allows the samples to be loaded simply by placing them into the resonator through special openings in the metal cavity. In this way, the measurement procedure is simplified, and the fixture/sample assembling time is reduced. We focused on the design of a fixture optimized for the characterization of materials with $1.5 < \varepsilon'_r < 5$ and high losses, $\tan\delta \sim 10^{-2}$. These values for ε'_r and $\tan\delta$ typically include soft substrates and materials used in additive manufacturing (AM) for high-frequency applications.

Due to the high e.m. losses of the materials under investigation, the best measurement sensitivity to the material $\tilde{\varepsilon}_r$ is obtained by limiting the volume of the dielectric sample to avoid a detrimental lowering of the fixture quality factor Q. A preliminary study focused on the optimization of the sample volume as a function of both ε'_r and ε''_r of the sample itself was shown in [13].

The presented fixture allows for $\tilde{\varepsilon}_r$ measurements of solid and relatively thick dielectric materials between 1 and 2 mm.

In particular, the measurement specifications and constraints addressed in this work are: 1) the need to characterize samples without disassembling the fixture, to simplify and speed up the user's operations; 2) the need to characterize thick (>1 mm) dielectric samples even at high frequencies (>10 GHz); and 3) the possibility to measure $\tilde{\varepsilon}_r$ of dielectric materials provided on planar metal backing plates. The possibility of characterizing thick samples is fundamental for the $\tilde{\varepsilon}_r$ measurement of typically used electronic substrates (e.g., FR4-fiberglass) which are generally provided with this thickness and, when needed, directly deposited on conductive ground planes. To the best of our knowledge, currently existing resonant fixtures are not able to fulfill all these measurement specifications simultaneously. For example, split post resonators (SPRs), which guarantee the highest $\tilde{\varepsilon}_r$ measurement accuracy [2], [14] for low-loss dielectric materials, are not suitable for thick samples and cannot work with dielectric samples grown on metal plates [14], [15], [16]. The metal plate also prevents the use of Cohn resonators [17], cylindrical-radial resonators [18], sheet resonators [19], standard configurations of the DRs [20], [21], and coaxial surface-wave resonators [22]. Thus, this work aims to fill the current lack of measurement instrumentation capable of satisfying the aforementioned requirements, in view of the importance that the characterization of dielectric materials is increasingly acquiring, thanks both to the development of new high-frequency technologies (e.g., 5G [23], 60-GHz radar sensors [24]) and also to the rapid diffusion of new materials, as those used in AM techniques, in radio frequency (RF) and higher-frequency applications [25].

To compare the techniques in a wide range of $\tilde{\varepsilon}_r$ values, we printed, with photopolymer materials through the PolyJet [26] deposition technique, different artificially porous samples with different air volumes. In this way, with a single material, we obtained samples with effective dielectric permittivity $1.7 < \varepsilon_r' < 3.1$ and $0.02 < \varepsilon_r'' < 0.06$ [27].

The new configuration of the DR shown in this article is experimentally validated through the comparison of $\tilde{\varepsilon}_r$ measurements obtained on the same materials with the well-known split ring resonator (SRR) method [28], [29], [30], [31], [32]. In particular, the SRR used for this validation is tuned at $\sim$2.2 GHz. Since SRRs generally operate at lower frequencies than that used by volume resonators as the DR, before performing this comparison, we experimentally verified the negligible frequency dependence (between 2 and 12 GHz) of ε_r' of the material family under investigation, through the use of a standard reflection/transmission technique using WR430 (at $\sim$2 GHz) and WR90 (at $\sim$12 GHz) waveguides. In addition to this, ε_r' measurements performed both with the SRR and waveguides on low-density polyvinylchloride (LD-PVC), polytetrafluoroethylene (PTFE), polymethyl methacrylate (PMMA), and polycarbonate (PC) were compared to verify the goodness of the calibration of the SRR. Thus, the SRR has been used to validate the DR by measurement comparisons.

The article is organized as follows. In Section II the measured samples are described. In Section III, we describe the proposed DR configuration, the measurement technique and method, the used system, and the obtained results. Then, in

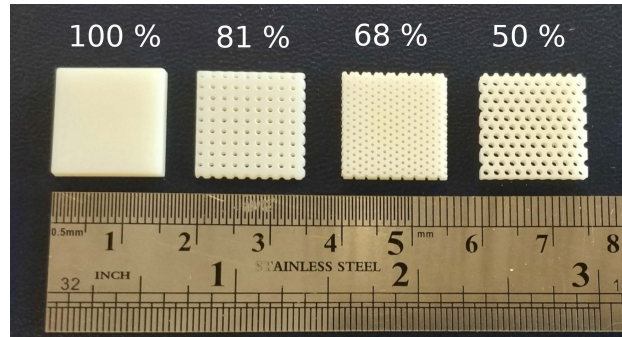| lattice type	l_p(mm)	$\varnothing_h$ (mm)	filling %
-	-	-	100
square	1.60	0.40	81
hexagonal	1.00	0.30	68
hexagonal	1.50	0.56	50

Fig. 1. Picture of the printed samples prepared for the DR, with the four different filling factors: 100%, 81%, 68%, and 50%.

Section IV, the DR experimental validation is discussed starting from the description of the used SRR and its calibration check through the waveguides measurements. Finally, in Section V, we comment on the obtained results, and a brief concluding summary is given in Section VI.

II. SAMPLES PREPARATION

The samples measured in this work were printed with a Stratasys[1] Objet30 PolyJet 3-D-printer using the high-temperature-resistant photopolymer RGD52 material and the SUP706 support [33].

The density of the samples, and thus their effective complex permittivity according to the theory for effective media [34], [35], was controlled by printing empty circular holes crossing the samples volume and arranged in various lattices with different filling factors. Hexagonal and square lattices were designed with different lattice parameters l_p and hole diameters $\varnothing_h$. All samples were prepared with $l_p \ll \lambda$, with λ being the wavelength in the medium, so that the samples are electromagnetically homogeneous enabling the use of an effective permittivity.

In Table I, we report the filling factors and the lattice features of the prepared samples.

For each density, samples with different physical dimensions were printed to fulfill the needs of DR and SRR measurement fixtures. For the DR, small and thin square samples with nominal side $L = 15.00$ mm were printed with different nominal thicknesses: 1.50 mm, 1.75 mm, and 2.00 mm. A picture of the samples printed for the DR is shown in Fig. 1. The samples for the SRR must be large enough to cover the whole surface of the resonator and must be thick enough to avoid leakage of the e.m. field out of the sample. Therefore, parallelepiped samples of size 40 mm $\times$ 40 mm $\times$ 30 mm were prepared. The samples were made by printing several layers of smaller

[1]Registered trademark.

height (2 mm) to reach a total height of 30 mm. This path was chosen since, by printing these large samples as a whole, manufacturing errors emerged, as a progressive misalignment of the circular holes. To prepare all the samples in the same way, the solid sample was obtained as a stack too. The layers were then stacked in a polystyrene support (see Fig. 6).

III. MEASUREMENT METHOD AND SYSTEM

In this section, we describe the proposed DR measurement configuration and discuss the measurement method. The section is articulated as: A) measurement method, B) measuring system, and C) measurement procedure and uncertainty evaluation.

A. Measurement Method

Since $\tilde{\varepsilon}_r$ of all the dielectric components loaded inside the resonator determines the amounts of the stored and dissipated energy, both the resonance frequency f_0 and the quality factor Q are sensitive to $\tilde{\varepsilon}_r$ [2]. Hence, $\tilde{\varepsilon}_r$ can be determined through their measurement.

The volume perturbation approach is used [2], [9]: a part of the inner volume of the resonator is filled with the sample under measurement keeping all the other parameters unchanged. Thus, in the small perturbation limit, the variation of the relative permittivity $\Delta\tilde{\varepsilon}_r = \Delta\varepsilon'_r - i\Delta\varepsilon''_r$ of a small volume of the resonator determines a change in the resonance frequency $\Delta f_0 \propto \Delta\varepsilon'_r$ and in the quality factor $\Delta(Q^{-1}) \propto \Delta\tan\delta$ [2]. Here, $\Delta x = x - x_{\text{ref}}$ denotes the variation of the parameter x with respect to a reference value x_{ref}.

In real cases, the required measurement sensitivity imposes a volume of the dielectric sample larger than the one compatible with the small perturbation limit. Thus, the change in ε'_r of the volume of the resonator filled with the sample changes the field configuration inside the resonator. Thus, even if the e.m. properties and size of all the other components of the resonator are kept fixed, their contribution to f_0 and Q changes due to the altered field configuration. Hence, the relationship between the sample properties (i.e., $\tilde{\varepsilon}_r$) and the resonator response (i.e., Q and f_0) is no more linear. A full e.m. simulation is thus used to obtain the calibration curve $\Delta f_0(\Delta\varepsilon'_r)$ through which $\varepsilon'_r = \Delta\varepsilon'_r + \varepsilon'_{\text{ref}}$ is determined from the measurement once the reference $\varepsilon'_{\text{ref}}$ is known.

Knowing ε'_r, the e.m. field configuration inside the resonator can be computed, as well as all the geometrical and filling factors, either analytically or through e.m. simulations, as done in this work. Then, it is possible to demonstrate [2], [13], [36] that

$$\Delta(Q^{-1}) = \sum_i R_i \Delta(G_i^{-1}(\varepsilon'_r)) + \Delta(\eta_d(\varepsilon'_r))\tan\delta_d$$
$$+ \Delta(\eta_s(\varepsilon'_r)\tan\delta_s) \quad (1)$$

with R_i and G_i being the surface resistance and the geometrical factor, respectively, of the ith metal surface of the cavity, $\tan\delta_d$ the loss tangent and η_d the filling factor of the dielectric parts of the DR distinct from the sample.

1. sample holder
2. lid
3. sample
4. dielectric crystal
5. lateral wall
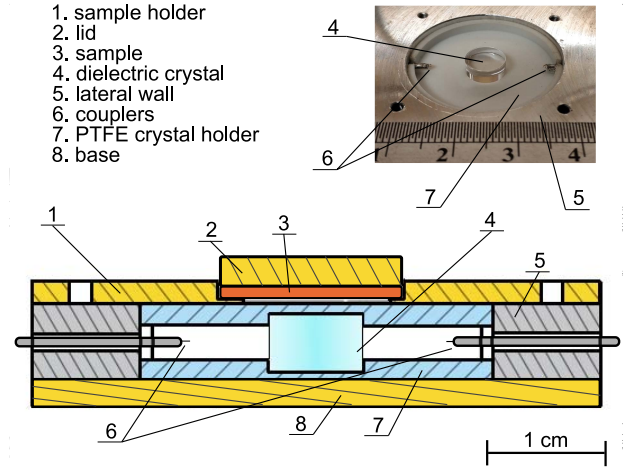6. couplers
7. PTFE crystal holder
8. base

Fig. 2. Top right: picture of the open cavity of the DR. Bottom: vertical section of the DR. The sample is placed between the sample holder and the lid. The TE$_{011}$ resonating mode is excited in the cavity through the couplers. The resonator quality factor is $Q \sim 5000$ without the sample. The base, the lid, and the sample holder are made of brass, and the lateral wall is in aluminum.

Finally, $\Delta(\eta_s\tan\delta_s) = \eta_s\tan\delta_s - \eta_{\text{ref}}\tan\delta_{\text{ref}}$ is the variation on the measured Q^{-1} caused by the substitution of the reference (subscript ref) with the sample (subscript s) under study. In particular, if the reference has $\tan\delta_{\text{ref}} = 0$ (e.g., vacuum) and the perturbation is small (i.e., $\Delta(G_i^{-1})$ and $\Delta\eta_v$ are negligible), the small perturbation limit approximation $\Delta(Q^{-1}) \sim \eta_s\tan\delta_s$ is recovered.

B. Measurement System

The straight vertical section of the used DR is shown in Fig. 2. It is composed of an aluminum cylindrical enclosure (height $h = 6.50(1)$ mm and diameter $\varnothing = 30.00(1)$ mm) loaded with a sapphire single crystal ($h = 5.00(1)$ mm, $\varnothing = 8.00(1)$ mm). The lid of the resonator can be opened for the insertion of the dielectric sample. The sample is held by a brass sample holder with a central hole of diameter $\varnothing = 13.00(1)$ mm. The TE$_{011}$ resonating mode is magnetically coupled in the cavity at $\sim$12.9 GHz.

The transmission S_{21} scattering parameter between the two ports of the DR is acquired with an Anritsu 37269D vector network analyzer (VNA) and the obtained resonance curve fit with the complex modified Lorentzian model [9], [37], [38], [39], [40]

$$S_{21} = \left(\frac{S_{21}(f_0)}{1 + i2Q\frac{f-f_0}{f_0}} + S_{\text{CC}}\right) e^{i(\alpha+\beta f)} \quad (2)$$

where S_{CC} is a complex parameter which represents the cross-coupling between the resonator couplers and $(\alpha + \beta f)$ is a phase delay term. Thus, this model takes into account typical non-idealities, which make the measured resonance curves asymmetric (Fig. 3). By using this generalized model, the accuracy and precision of the Q and f_0 measurements are increased [9], [37], [41].
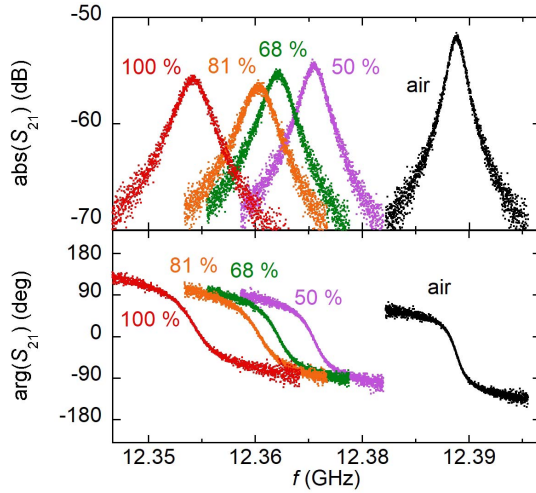
Fig. 3. Example of the absolute value abs(S_{21}) and argument arg(S_{21}) of the transmission scattering parameter S_{21} measured with the DR on 2-mm thick samples with 100% (red), 81% (orange), 68% (green), 50% (purple), and 0% (black) filling factors.

Fig. 4. Blue lines are the computed variations of the resonance frequency Δf_0 as a function of the sample thickness for different ε'_r values. The full dots represent the experimental data obtained on the full (100%) sample (red dots) and the 81% (orange squares), 68% (green rhombi), and 50% (purple triangles) filled samples.

C. Measurement Procedure and Uncertainty Evaluation

In this section, the measurement procedure, the uncertainty analysis, and the measurement results obtained with the DR are reported.

For each sample, ten different mountings were performed and for each mounting, ten acquisitions of the resonator scattering parameters were performed with 1601 points evenly spaced in frequency. During a frequency sweep, every point was averaged over five acquisitions. The frequency span was chosen to be ~5 full-width half-maximum (FWHMs) of the resonance curve to keep the point density fixed in every acquisition and to reduce the measurement uncertainties on the resonating parameters, as extensively described in [39]. The selected frequency span improves the determination of the complex cross-coupling factor S_{CC} and of the phase delay term, increasing in this way the accuracy of the Q and f_0 measurements in asymmetric resonance curves [39].

The relative standard deviation on f_0 obtained from the different mountings was $u_m(f_0)/f_0 < 10^{-6}$ including the measurement repeatability and the fit precision. Since we need to associate to each sample thickness the measured f_0, we propagated on the overall $u(f_0)$ and also the uncertainty $u(t)$ on the sample thickness t. The uncertainty on f_0 caused by $u(t)$ is $u_t(f_0) = u(t)\partial f_0/\partial t$. The sensitivity function $\partial f_0/\partial t$ was evaluated with e.m. simulations and $u(t)$ was evaluated as the standard deviation of ten different t measurements performed with a micrometer on each sample. Thus, $u^2(f_0) = u_m^2(f_0) + u_t^2(f_0)$.

To implement the perturbative approach, reference measurements must be performed as explained in Section III-A. For this purpose, the volume occupied by the sample under measurement must be substituted by the same volume of air, so that $\tilde{\varepsilon}_{ref} = \varepsilon'_{air} \approx 1$ and $\tan \delta_{ref} = \tan \delta_{air} \approx 0$. The above approximations can be done since the sensitivity limits of the measurement method prevent distinguishing the dielectric properties of air from those of vacuum [13]. Hollow rings, printed with the same thickness as the samples and with inner
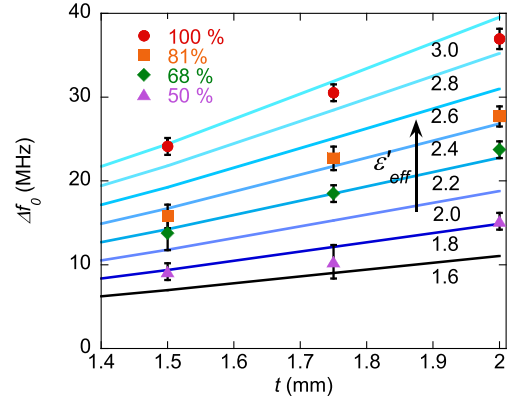
diameter $\varnothing \sim 14$ mm (which is larger than the sample holder hole), are used as spacers once loaded below the DR lid, providing the same gap between the lid and the dielectric puck in both the reference and the sample measurements. The e.m. properties of the material of the ring are irrelevant to the measurement since the ring is set far enough from the volume where the e.m. mode extends. With this procedure, the measured variation of the resonance frequency $\Delta f_0 = f_{0,ref} - f_{0,s}$ can be entirely attributed to the change in $\tilde{\varepsilon}_r$ of the probed volume and not to variations in the DR geometry. In the above, the resonance frequencies $f_{0,ref}$ and $f_{0,s}$ are those measured with the DR loaded with the ring (reference) and with the sample, respectively. The uncertainty of Δf_0 was obtained from $u^2(\Delta f_0) = u^2(f_{0,ref}) + u^2(f_{0,s})$.

The experimental points for Δf_0 were reported on the calibration curves (obtained through e.m. simulation of the DR) shown in Fig. 4: it can be noticed that samples of different thicknesses but of the same filling factor are placed, within a good approximation, on the same $\Delta f_0(t, \varepsilon'_r)$ curve. For a better evaluation of ε'_r, the calibration curves shown in Fig. 4 were cut at fixed t values, thus obtaining the $\varepsilon'_r(\Delta f_0)$ curves shown in Fig. 5. In this figure, the data points for Δf_0 measured on the full sample are reported as an example: it can be noted that the 1σ probability intervals of the obtained ε'_r at different thicknesses overlap. The best estimation of ε'_r for the (full) samples of different thicknesses was obtained from the average of their ε'_r values, and the uncertainty was evaluated with the standard propagation procedure on the calculus of the averages [42].

The imaginary part ε''_r of the relative permittivity was then obtained as $\varepsilon''_r = \tan \delta_s \varepsilon'_r$ from Q measurements using (1), with $R = 92(12)$ mΩ and $\tan \delta_v = 4(2) \times 10^{-5}$ evaluated with a calibration procedure based on the round robin rotation technique [43]. The uncertainties $u(\varepsilon''_r)$ were finally obtained from (1) with the standard uncertainty propagation procedure [42]: $u(Q)/Q = 1\%$, which includes the mounting repeatability; $u(G)$ and $u(\eta)$ were obtained through e.m. simulations with the Monte Carlo method by varying all the physical dimensions and e.m. properties of the components
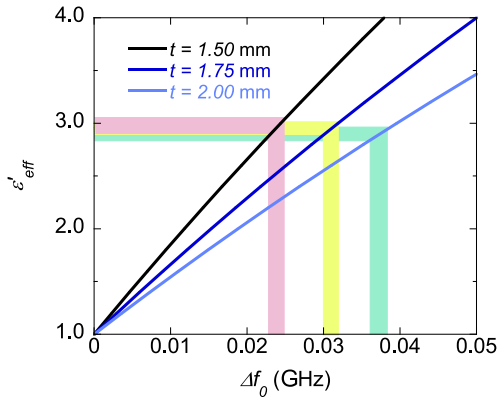
Fig. 5. Experimental Δf_0 with their 1σ probability intervals measured on the 1.50 mm (light red area), 1.75 mm (yellow area), and 2.00 mm (green area) are reported and converted to the experimental ε_r' through the calibration curves $\varepsilon_r'(\Delta f_0)$ computed for samples of thicknesses 1.50 mm (black curve), 1.75 mm (dark blue curve), and 2.00 mm (light blue curve).

of the resonator in their variability intervals [44]; $u(R)$ and $u(\tan \delta_v)$ are those above reported.

The measurement results are shown in Fig. 7 and will be commented in Section V, together with the results of the Section IV.

IV. EXPERIMENTAL VALIDATION

In this section, we discuss the experimental validation of the here presented measurement fixture. Since at these frequencies, there are no $\tilde{\varepsilon}_r$ measurement standards (neither solid nor liquid), and it was not possible to directly check the DR measurement performances through the use of known materials. For this reason, we compared the measurement results obtained with the DR with those provided on the same material by a SRR tuned at ~2.2 GHz. In addition to this, as a further validation, the calibration of the used SRR was checked through the comparison of ε_r' measurements performed on LD-PVC, PTFE, PMMA, and PC both with the SRR and with the standard reflection/transmission method based on the NIST variation of the Nicolson–Ross–Weir method [45]. The reflection/transmission measurements were performed with WR430 and WR90 waveguides to show the frequency independence of the e.m. properties of this class of dielectrics in the operative frequency range of the DR and the SRR.

We first describe the used SRR, then we show the comparison with the waveguide measurements, and finally we show and compare the results obtained with the DR on the samples described in Section II.

A. Split-Ring Resonator

The SRR consists of metal tracks etched on the top of a dielectric substrate and a metal ground, placed on the bottom part (Fig. 6). The tracks consist of two concentric rings, known as *circular crowns*, that present two diametrically opposed cuts, hence the name of the resonator, that is, "split" ring resonator [46]. On the ring sides, there are two microstrip-feeding lines of larger thickness with respect to the rings, while another smaller microstrip line, aligned
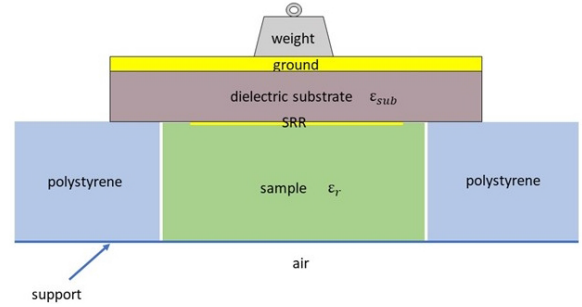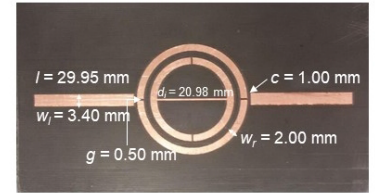

Fig. 6. Top right: picture of the SRR. Bottom: vertical section of the SRR. The sample was placed below and in contact with the resonator and a certified mass of 1 kg placed on the other side (ground layer) to ensure good adherence of the sample and constant pressure in all the measurements.

with the feeds, is placed along the diameter of the innermost circular crown. The chosen substrate is Duroid[1] RT-5870, with nominal thickness $t_s = 1.19$ mm, relative permittivity $\varepsilon_{sub} = 2.33(2)$, loss tangent $\tan \delta \simeq 0.0012$, nominal copper thickness $t_c = 35$ μm, and a total substrate dimension of 68.000(5) mm × 100.000(5) mm. The SRR is accessible through two coaxial connectors, coupled to the feeding lines, which are located on the bottom part of the structure.

The resonance frequency f_0 depends on the geometry of the SRR; modeling the structure as an LC circuit [47], its f_0 is given by $f_0 = 1/(2\pi \sqrt{LC})$. The overall geometry was simulated and optimized by the e.m. software CST Microwave Studio[1]. Due to the well-defined geometry of the couplers in the SRR, the simulated quantity is the directly loaded Q-factor Q_l of the resonator. The final simulated resonance frequency in the air is approximately 2.22 GHz with $Q_l \sim 140$. Once the SRR was realized and tested in air, the size and the e.m. parameters of the simulation model were tuned, within the size uncertainties of the components of the SRR, through a multidimensional optimization, to minimize the differences between the simulated f_0 and Q_l and the measured ones.

If the SRR works with a dielectric sample having complex relative permittivity $\tilde{\varepsilon}_r$ in contact with the resonator, as shown in Fig. 6, its resonance frequency and quality factor are affected. Performing a series of CST[1] simulations with ε_r' varying between 1 and 10, it was possible to evaluate the relationship between resonance frequency shift (Δf_0) and the sample permittivity (ε_r'). The numerically obtained data were found to be best fit through a second-order polynomial yielding the following calibration equation:

$$\varepsilon_r' = 1.00 + 3.64\Delta f_0 + 11.93(\Delta f_0)^2 \qquad (3)$$

where f_0 is in GHz. Therefore, by performing f_0 measurements in the presence of a sample, it is possible to evaluate its relative permittivity ε_r'. For what concerns $\tan \delta$ of the sample,

TABLE II

MEASUREMENTS OF ε_r' ON CONTROL SAMPLES.
STANDARD UNCERTAINTIES ARE REPORTED

material	ε_r' - SRR	ε_r' - WR430	ε_r' - WR90
LD-PVC	1.6(1)	1.62(3)	1.61(2)
PTFE	1.9(1)	2.06(4)	2.04(2)
PMMA	2.4(1)	2.59(5)	2.59(3)
PC	2.7(1)	2.82(6)	2.81(3)

we observed a linear dependence of the inverse of the SRR quality factor

$$\tan \delta(Q_l^{-1}) = p_1 Q_l^{-1} + p_2. \qquad (4)$$

However, it must be noticed that the calibration curve $\tan \delta(Q_l^{-1})$ depends on ε_r' of the sample. Thus, through e.m. simulations, the dependencies of the coefficients $p_1(\varepsilon_r')$ and $p_2(\varepsilon_r')$ were obtained by varying ε_r' in the interval 1–10 in steps of 1. The obtained points fit with the following functions:

$$p_1 = 6.54\varepsilon_r'^{-0.60} \qquad (5)$$

$$p_2 = -0.0010\varepsilon_r'^2 + 0.010\varepsilon_r' - 0.048. \qquad (6)$$

The determination coefficients of (5) and (6) are $r^2 = 0.998$ and $r^2 = 0.974$, respectively. Thus, once the sample ε_r' is determined using the measured Δf_0 with (3), p_1 and p_2 are determined and then $\tan \delta$ obtained through the measured Q_l with (4).

The measurement system is shown in Fig. 6. The SRR is placed in contact with and on top of the sample to be measured, which is in turn kept in place by a holder. This holder is made of polystyrene, so as not to affect the resonance frequency of the system. To force the SRR to adhere to the sample, exercising always the same force, a certified mass of 1 kg was used. This enhances the measurement repeatability [48]. The transmission scattering parameter S_{21} is acquired through a PNA network analyzer, model E8363C, Agilent Technologies, with a 100-kHz sampling step, a 3-kHz resolution bandwidth, and -20 dBm source power. A vector error correction procedure is preliminarily performed, employing the N4691B Ecal kit.

B. Comparison With Transmission/Reflection Methods

The calibration curves obtained through the e.m. simulation of the SRR are experimentally verified by testing the SRR on the following materials: LD-PVC, PTFE, PMMA, and PC. These samples were characterized with the SRR and, for comparison, with the standard reflection/transmission technique, based on the NIST method [45], through WR430 (at ∼2 GHz) and WR90 (at ∼12 GHz) waveguides [49]. The results are shown in Table II.

The SRR and the WR430 systems provide comparable ε_r' on all the tested materials at the same working frequencies. The results obtained on PTFE, PMMA, and PC are also well in agreement with [20]. The agreement of the measurements obtained with the WR430 and the WR90 waveguides experimentally demonstrates the negligible ε_r' frequency dependence of this class of materials up to ∼12 GHz. This validates directly the SRR method (at least for ε_r' measurements) and
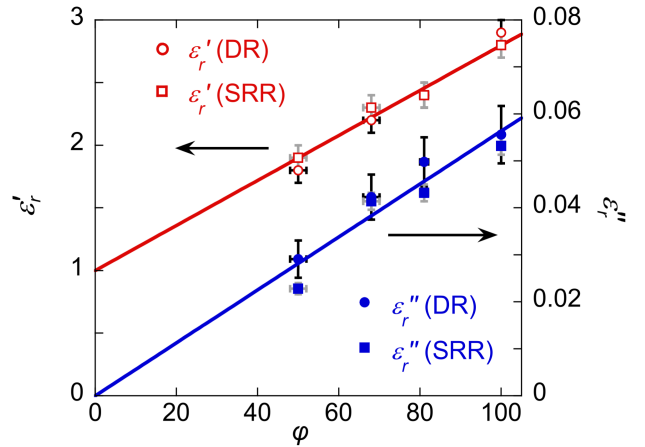

Fig. 7. Real part ε_r' (red empty symbols) and imaginary part ε_r'' (blue full symbols) of the complex dielectric permittivity of the samples measured with the DR (circles) and with the SRR (squares) as a function of the filling percentage φ. The ε_r' points measured with the DR and the SRR overlap. The straight lines are obtained from the linear fit of the measured data once the completely empty sample (air) constraints are fixed: $\varepsilon_r' \to 1$, $\varepsilon_r'' \to 0$ for $\varphi \to 0\%$.

legitimates the comparison between the SRR and the DR despite the different operative frequencies.

C. Comparison With the DR

Once the calibration of the SRR is experimentally verified, the SRR can be used to validate the DR by a comparison of $\tilde{\varepsilon}_r$ measurement performed on the same materials. In this work, to compare the techniques in a sufficiently wide $\tilde{\varepsilon}_r$ values space, test samples are printed with different infill percentages as discussed in Section II.

For each sample, with the SRR, ten repetitions were performed, each time removing the SRR and the sample from the polystyrene holder. A preliminary measurement in the air was performed, with the empty holder, to provide the reference for the evaluation of the resonance frequency shift due to the sample. The type-A standard uncertainty related to the measurement repeatability was then combined with the uncertainty given by the curve fitting algorithm $(u(Q_l)/Q_l < 10^{-4}$ and $u(f_0)/f_0 < 6 \times 10^{-7})$ and then straightforwardly propagated to the measured permittivity using (3) and (4). A further uncertainty contribution related to the fitting of the calibration function to the numerically simulated data must also be taken into account. From the residuals of the fitting on the ten simulation points, $u(\varepsilon_r') \sim 0.1$ can be assessed through (3). The same kind of source of uncertainty is also taken into account for the evaluation of $\tan \delta$ from (4) through (5) and (6). We note that the above-reported uncertainty is the dominant term as compared to the contribution obtained from the propagation of the standard uncertainty of the measured resonance frequency shift.

The final results in terms of measured permittivity for the different samples are reported in Fig. 7.

V. RESULTS AND DISCUSSION

In Fig. 7, the data for $\tilde{\varepsilon}_r$ measured with both resonators are reported as a function of the percentage-filling factor of

the sample φ. The experimental data for ε'_r are well fit by the linear function $\varepsilon'_r(\varphi) = (\varepsilon'_r(100\%) - 1)\varphi/100 + 1$, while the imaginary part with $\varepsilon''_r(\varphi) = \varepsilon''_r(100\%)\varphi/100$. The points $\varepsilon'_r(0\%) = 1$, $\varepsilon''_r(0\%) = 0$ are constrained by the values of air. The linear dependence of the measured points is well in agreement with the upper limit of the Wiener model for the effective medium theory [34], [35] as already observed in [50] and [51] for the effective values of ε'_r, and also for ε''_r [52]. From the slopes of the linear fits, we obtain $\tilde{\varepsilon}_r(100\%) = 2.80(5) - i0.057(2)$ for the full sample. The standard complex uncertainty $u(\tilde{\varepsilon}_r(100\%))$ is evaluated from the linear fit with the Monte Carlo method assuming all the $u(\tilde{\varepsilon}_r(\varphi))$ and $u(\varphi)$ to be Gaussian and centered [44]. $u(\varphi)$ is obtained starting from the linear printing precision declared by the manufacturer of the 3-D-printer (i.e., ~ 0.01 mm) [33] and propagating this uncertainty on φ taking into account the geometry of the samples. We notice that $\tilde{\varepsilon}_r(100\%)$ measurement is in good agreement with literature [53], [54]. For what concerns the measurement uncertainty comparison of the new DR configuration with other measurement techniques, we can assess that the technique proposed in this work is aligned with the typical uncertainty levels of this kind of measurement. In [54], the complex $\tilde{\varepsilon}_r$ of acrylonitrile butadiene styrene (ABS) samples doped with different amounts of BaTiO$_3$ microparticles was measured by means of a split-post dielectric resonator (SPDR) with a nominal resonance frequency of 15 GHz. SPDR is well known to be one of the most accurate methods for the measurement of planar dielectric samples [2], [14]. In [54] uncertainties $u(\varepsilon'_r)/\varepsilon'_r \sim 1\%$ (including systematic contributions) and $u(\tan\delta)/\tan\delta \sim 0.2\%$ (evaluated as the standard deviation of six measurements) were reported. In [20], bulk ABS samples were measured at 10 GHz with a dielectric resonator, giving at room temperature $u(\varepsilon'_r)/\varepsilon'_r \sim 1\%$ and $u(\tan\delta)/\tan\delta \sim 20\%$. Broadband techniques were also used although, as previously stated, they are usually less sensitive and accurate than resonant methods [2]. In [53], a Nicholson–Ross–Weir waveguide method was used in the 8.2–11-GHz band on a wide variety of 3-D printing materials obtaining a maximum standard deviation for the set of ABS samples $u(\varepsilon'_r)/\varepsilon'_r \leq 5.8\%$ and an approximate range of estimated errors 10%–300% on $\tan\delta$, although a complete uncertainty analysis in this frequency band was not presented.

Therefore, the new configuration of the showed DR allows the characterization of samples with geometries and sizes difficult to characterize in other ways and with uncertainties aligned with the current state of the art.

The obtained results from the DR and the SRR are almost the same despite the different working frequencies. Even the uncertainties given by both techniques are the same despite the SRR being much more sensitive to ε'_r of the material under investigation than the DR. The sensitivity of the SRR f_0 to ε'_r variations is estimated to be $\partial\Delta f_0/\partial\varepsilon'_r \sim 112$ MHz at $\varepsilon'_r = 2.4$ while that of DR, from Fig. 4, ~ 20 MHz in the same conditions and with the thickest sample ($t = 2$ mm). This is an expected result since both SRR and DR are based on volume perturbation, so that the SRR is favored by the use of thicker (bulk) dielectric samples. However, the typical final uncertainty is the same for both techniques, since $u(f_0)/f_0$ is

much smaller for the DR thanks to its higher quality factor $2500 < Q < 5000$ in the conditions of the measurements here presented.

A final remark should be made about a possible anisotropy of printed samples. Using a waveguide reflection method, a uniaxial anisotropy factor of $\sim 7\%$ was measured on ε'_r of 3-D-printed polylactide acid (PLA) samples at 40 GHz [55]. The samples were produced with the standard printing procedure, based on the extrusion and deposition of fused filaments. Such printing technique generates anisotropic structures due to the discrete and weakly connected printed layers [55], as also shown in [56]. On the contrary, for the realization of the samples here studied, a PolyJet printer was used: the material is deposited in liquid form and then polymerized with UV-rays. Thus, one expects a tighter connection between the printed layers, with a reduced amount of defects and an overall reduced anisotropy. The resulting anisotropy level is then believed to be well below $u(\varepsilon'_r)$ and $u(\varepsilon''_r)$. In addition, the DR is excited in a quasi-TE$_{011}$ mode and thus the electric field vector is, within a good approximation, directed along the printing layers. In the SRR, instead, the electric field direction is not directed along some preferred e.m. direction of the sample. Since no evident difference was measured on $\tilde{\varepsilon}_r$ with both resonators, we conclude that the small anisotropy of the samples, including the contribution given by the aligned holes, does not affect the results presented.

At the end of the calibration and validation procedure of this new configuration of DR, we can reliably use this fixture for the characterization of other substrates materials. We measured $\tilde{\varepsilon}_r$ of a FR-4 fiberglass substrate with copper ground plane obtaining $\varepsilon'_r = 4.76(8)$ and $\tan\delta = 1.73(6) \times 10^{-2}$ fairly in agreement with [57] and [58]. We also tested the DR with Kapton[1] polyimide stacking ten layers of 127-μm-thick films and obtaining $\varepsilon'_r = 4.01(5)$ and $\tan\delta = 9.9(2) \times 10^{-3}$ in good agreement with [59]. These comparisons with the literature further validate the proposed fixture.

VI. SUMMARY

We have demonstrated the application of a DR to the measurement of the complex relative permittivity $\tilde{\varepsilon}_r$ of dielectric samples printed with a PolyJet 3-D-printer. The 3-D printing technique allowed us to obtain samples with different filling factors, to vary the effective relative permittivity $\tilde{\varepsilon}_r$ in a geometrically controlled way. The dependence of $\tilde{\varepsilon}_r$ on the density of the sample was found to be well described by the Wiener upper bound in agreement with [50], [51], and [52]. The measurement technique was validated by comparing the $\tilde{\varepsilon}_r$ measurements performed with an SRR.

In conclusion, the obtained results demonstrated the possibility to employ a DR for microwave $\tilde{\varepsilon}_r$ characterization of 3-D printing materials, and soft substrates for electronic circuits with similar e.m. characteristics even in the presence of back metal ground plates.

REFERENCES

[1] U. Kaatze, "Techniques for measuring the microwave dielectric properties of materials," *Metrologia*, vol. 47, no. 2, pp. S91–S113, Apr. 2010.

[2] L.-F. Chen, C. Ong, C. Neo, V. Varadan, and V. K. Varadan, *Microwave Electronics: Measurement and Materials Characterization*. Hoboken, NJ, USA: Wiley, 2004.

[3] J. Krupka and C. Weil, "Recent advances in metrology for the electromagnetic characterization of materials at microwave frequencies," in *Proc. 12th Int. Conf. Microw. Radar (MIKON)*, vol. 4, May 1998, pp. 243–253.

[4] E. J. Vanzura, J. R. Baker-Jarvis, J. H. Grosvenor, and M. D. Janezic, "Intercomparison of permittivity measurements using the transmission/reflection method in 7-mm coaxial transmission lines," *IEEE Trans. Microw. Theory Techn.*, vol. 42, no. 11, pp. 2063–2070, 1994.

[5] C. M. Weil, M. D. Janevic, and E. J. Vanzura, "Intercomparison of permittivity measurements using the transmission/reflection method in 7 and 14-mm coaxial air lines," Nat. Inst. Standard Technol. (NIST), Gaithersburg, MD, USA, Tech. Rep. 1386, 1997.

[6] *Electronic Characteristic Measurements—Surface Resistance of High-temperature Superconductors at Microwave Frequencsies*, International Electrotechnical Commission, Standard IEC 61788-7:2020, Mar. 2020.

[7] Y. Kobayashi, T. Imai, and H. Kayano, "Microwave measurement of temperature and current dependences of surface impedance for high-T_c superconductor," *IEEE Trans. Microw. Theory Techn.*, vol. 39, no. 9, pp. 1530–1538, Sep. 1991.

[8] J. Mazierska and C. Wilker, "Accuracy issues in surface resistance measurements of high temperature superconductors using dielectric resonators (corrected)," *IEEE Trans. Appl. Supercond.*, vol. 11, no. 4, pp. 4140–4147, Dec. 2001.

[9] A. Alimenti, K. Torokhtii, E. Silva, and N. Pompeo, "Challenging microwave resonant measurement techniques for conducting material characterization," *Meas. Sci. Technol.*, vol. 30, no. 6, Jun. 2019, Art. no. 065601.

[10] A. Alimenti et al., "Microwave measurements of the high magnetic field vortex motion pinning parameters in Nb_3Sn," *Superconductor Sci. Technol.*, vol. 34, no. 1, 2020, Art. no. 014003.

[11] N. Pompeo et al., "Intrinsic anisotropy and pinning anisotropy in nanostructured $YBa_2Cu_3O_7$ from microwave measurements," *Superconductor Sci. Technol.*, vol. 33, no. 4, 2020, Art. no. 044017.

[12] N. Pompeo, A. Alimenti, K. Torokhtii, G. Sylva, V. Braccini, and E. Silva, "Microwave properties of Fe (Se,Te) thin films in a magnetic field: Pinning and flux flow," in *Proc. J. Phys., Conf.*, 2020, vol. 1559, no. 1, Art. no. 012055.

[13] A. Alimenti, K. Torokhtii, N. Pompeo, E. Piuzzi, and E. Silva, "Characterisation of dielectric 3D-printingmaterials at microwave frequencies," *Acta IMEKO*, vol. 9, no. 3, pp. 26–32, 2020.

[14] J. Krupka, A. P. Gregory, O. C. Rochard, R. N. Clarke, B. Riddle, and J. Baker-Jarvis, "Uncertainty of complex permittivity measurements by split-post dielectric resonator technique," *J. Eur. Ceram. Soc.*, vol. 21, no. 15, pp. 2673–2676, Dec. 2001.

[15] *Split Post Dielectric Resonators for Dielectric Measurements of Substrates*, Keysight Technologies, Santa Rosa, CA, USA, Appl. Note 5989-5384EN, Dec. 2017.

[16] J. Krupka, "Measurements of the complex permittivity of microwave circuit board substrates using split dielectric resonator and reentrant cavity techniques," in *Proc. 7th Int. Conf. Dielectric Mater., Meas. Appl.*, 1996, pp. 21–24.

[17] S. Cohn and K. Kelly, "Microwave measurement of high-dielectric-constant materials," *IEEE Trans. Microw. Theory Techn.*, vol. MTT-14, no. 9, pp. 406–410, Sep. 1966.

[18] W. R. Humbert and W. R. Scott, "A new technique for measuring the permittivity and loss tangent of cylindrical dielectric rods," *IEEE Microw. Guided Wave Lett.*, vol. 6, no. 7, pp. 262–264, Jul. 1996.

[19] G. Kent, "Dielectric resonances for measuring dielectric properties," *Microw. J.*, vol. 31, p. 99, 1988.

[20] B. Riddle, J. Baker-Jarvis, and J. Krupka, "Complex permittivity measurements of common plastics over variable temperatures," *IEEE Trans. Microw. Theory Techn.*, vol. 51, no. 3, pp. 727–733, Mar. 2006.

[21] J. Krupka, K. Derzakowski, A. Abramowicz, M. E. Tobar, and R. G. Geyer, "Use of whispering-gallery modes for complex permittivity determinations of ultra-low-loss dielectric materials," *IEEE Trans. Microw. Theory Techn.*, vol. 47, no. 6, pp. 752–759, Jun. 1999.

[22] A. Marincic, F. Benson, and J. Tealby, "Measurements of permittivity by the use of surface waves in open and closed structures," *IEE Proc. H Microw., Antennas Propag.*, vol. 133, no. 6, pp. 441–449, 1986.

[23] S. Zhang, "An overview of network slicing for 5G," *IEEE Wireless Commun.*, vol. 26, no. 3, pp. 111–117, Jun. 2019.

[24] Y. Li, C. Gu, and J. Mao, "4-D gesture sensing using reconfigurable virtual array based on a 60-GHz FMCW MIMO radar sensor," *IEEE Trans. Microw. Theory Techn.*, vol. 70, no. 7, pp. 3652–3665, Jul. 2022.

[25] A. Al Rashid, S. A. Khan, S. G. Al-Ghamdi, and M. Koç, "Additive manufacturing of polymer nanocomposites: Needs and challenges in materials, processes, and applications," *J. Mater. Res. Technol.*, vol. 14, pp. 910–941, Sep. 2021.

[26] C. Ulbrich et al., "Comparison of five rapid prototype techniques (SLS/FDM/DLP/3DP/Polyjet)," in *Proc. 5th Int. Conf. Adv. Res. And Rapid Prototyping*, Leira, Portugal, Sep. 2012, pp. 573–580.

[27] J. C. Maxwell, *A Treatise on Electricity and Magnetism*, vol. 1. Oxford, U.K.: Clarendon Press, 1881.

[28] S. P. Chakyar, S. K. Simon, C. Bindu, J. Andrews, and V. P. Joseph, "Complex permittivity measurement using metamaterial split ring resonators," *J. Appl. Phys.*, vol. 121, no. 5, Feb. 2017, Art. no. 054101.

[29] M. Saadat-Safa, V. Nayyeri, A. Ghadimi, M. Soleimani, and O. M. Ramahi, "A pixelated microwave near-field sensor for precise characterization of dielectric materials," *Sci. Rep.*, vol. 9, no. 1, pp. 1–12, Sep. 2019.

[30] H. Sun, R. Li, G. Y. Tian, T. Tang, G. Du, and B. Wang, "Determination of complex permittivity of thin dielectric samples based on high-q microstrip resonance sensor," *Sens. Actuators A, Phys.*, vol. 296, pp. 31–37, Sep. 2019.

[31] K. Xu et al., "Novel microwave sensors based on split ring resonators for measuring permittivity," *IEEE Access*, vol. 6, pp. 26111–26120, 2018.

[32] H.-R. Sun et al., "Symmetric coplanar waveguide sensor loaded with interdigital capacitor for permittivity characterization," *Int. J. RF Microw. Comput.-Aided Eng.*, vol. 30, no. 1, 2020, Art. no. e22023.

[33] *Stratasys Web Page*. Accessed: Sep. 21, 2021. [Online]. Available: https://www.stratasys.com/

[34] Z.-M. Dang, J.-K. Yuan, J.-W. Zha, T. Zhou, S.-T. Li, and G.-H. Hu, "Fundamentals, processes and applications of high-permittivity polymer–matrix composites," *Prog. Mater. Sci.*, vol. 57, pp. 660–723, May 2012.

[35] D. V. Isakov, Q. Lei, F. Castles, C. J. Stevens, C. R. M. Grovenor, and P. S. Grant, "3D printed anisotropic dielectric composite with metamaterial features," *Mater. Des.*, vol. 93, pp. 423–430, Mar. 2016.

[36] R. E. Collin, *Foundations for Microwave Engineering*. Hoboken, NJ, USA: Wiley, 2007.

[37] P. J. Petersan and S. M. Anlage, "Measurement of resonant frequency and quality factor of microwave resonators: Comparison of methods," *J. Appl. Phys.*, vol. 84, no. 6, pp. 3392–3402, Sep. 1998.

[38] K. Torokhtii, A. Alimenti, N. Pompeo, and E. Silva, "Estimation of microwave resonant measurements uncertainty from uncalibrated data," *Acta IMEKO*, vol. 9, no. 3, pp. 47–52, 2020.

[39] K. Torokhtii, A. Alimenti, N. Pompeo, and E. Silva, "Frequency span optimization for asymmetric resonance curve fitting," in *Proc. IEEE Int. Instrum. Meas. Technol. Conf. (I2MTC)*, May 2021, pp. 1–5.

[40] K. Torokhtii et al., "Q-factor of microwave resonators: Calibrated vs. uncalibrated measurements," in *Proc. J. Phys., Conf.*, vol. 1065, Aug. 2018, Art. no. 052027, doi: 10.1088/1742-6596/1065/5/052027.

[41] N. Pompeo, K. Torokhtii, F. Leccese, A. Scorza, S. Sciuto, and E. Silva, "Fitting strategy of resonance curves from microwave resonators with non-idealities," in *Proc. IEEE Int. Instrum. Meas. Technol. Conf. (I2MTC)*, May 2017, pp. 1–6.

[42] Joint Committee for Guides in Metrology, *Evaluation of Measurement Data—Guide to the Expression of Uncertainty in Measurement*, document JCGM 100, 2008.

[43] A. Alimenti, K. Torokhtii, N. Pompeo, and E. Silva, "Sensitivity limits comparison of surface resistance measurements based on dielectric loaded resonators," in *Proc. J. Phys., Conf.*, vol. 1065, 2018, Art. no. 052029.

[44] Joint Committee for Guides in Metrology, *Evaluation of Measurement Data—Supplement 1 to the Guide to the Expression of Uncertainty in Measurement—Propagation of Distributions Using a Monte Carlo Method*, document JCGM 101, 2008.

[45] J. Baker-Jarvis, E. J. Vanzura, and W. A. Kissick, "Improved technique for determining complex permittivity with the transmission/reflection method," *IEEE Trans. Microw. Theory Techn.*, vol. 38, no. 8, pp. 1096–1103, Aug. 1990.

[46] R. A. Alahnomi, Z. Zakaria, E. Ruslan, A. A. M. Bahar, and S. R. A. Rashid, "High sensitive microwave sensor based on symmetrical split ring resonator for material characterization," *Microw. Opt. Techn. Lett.*, vol. 58, pp. 2106–2110, Sep. 2016.

[47] J. D. Baena et al., "Equivalent-circuit models for split-ring resonators and complementary split-ring resonators coupled to planar transmission lines," *IEEE Trans. Microw. Theory Techn.*, vol. 53, no. 4, pp. 1451–1461, Apr. 2005.

[48] L. D'Alvia, E. Pittella, S. Pisa, E. Piuzzi, and Z. Del Prete, "Effect of applied pressure on patch resonator-based measurements of moisture level for cultural heritage materials," in *Proc. Metrol. Archaeol. Cultural Heritage (MetroArchaeo)*, Cassino, Italy, Oct. 2018, pp. 1–5.

[49] E. Piuzzi et al., "Measurement system for evaluating dielectric permittivity of granular materials in the 1.7–2.6-GHz band," *IEEE Trans. Instrum. Meas.*, vol. 65, no. 5, pp. 1051–1059, May 2016.

[50] H. Hu, S. Sinha, N. Meisel, and S. G. Bilén, "Permittivity of 3D-printed nylon substrates with different infill patterns and densities for design of microwave components," *Designs*, vol. 4, no. 3, p. 39, Sep. 2020.

[51] G. A. Ramirez Arroyave and J. L. Araque Quijano, "Broadband characterization of 3D printed samples with graded permittivity," in *Proc. Int. Conf. Electromagn. Adv. Appl. (ICEAA)*, Sep. 2018, pp. 584–588.

[52] A. Goulas et al., "Fused filament fabrication of functionally graded polymer composites with variable relative permittivity for microwave devices," *Mater. Des.*, vol. 193, Aug. 2020, Art. no. 108871.

[53] P. I. Deffenbaugh, R. C. Rumpf, and K. H. Church, "Broadband microwave frequency characterization of 3-D printed materials," *IEEE Trans. Compon., Packag., Manuf. Technol.*, vol. 3, no. 12, pp. 2147–2155, Dec. 2013.

[54] F. Castles et al., "Microwave dielectric characterisation of 3D-printed $BaTiO_3$/ABS polymer composites," *Sci. Rep.*, vol. 6, Mar. 2016, Art. no. 022714.

[55] J. M. Felicio, C. A. Fernandes, and J. R. Costa, "Complex permittivity and anisotropy measurement of 3D-printed PLA at microwaves and millimeter-waves," in *Proc. 22nd Int. Conf. Appl. Electromagn. Commun. (ICECOM)*, Sep. 2016, pp. 1–6.

[56] A. Goulas et al., "The impact of 3D printing process parameters on the dielectric properties of high permittivity composites," *Designs*, vol. 3, no. 4, p. 50, 2019.

[57] A. Raveendran and S. Raman, "Complex permittivity extraction of planar dielectrics using a noninvasive microwave transmission line resonant technique," *IEEE Trans. Instrum. Meas.*, vol. 70, pp. 1–8, 2021.

[58] A. R. Djordjevic, R. M. Biljie, V. D. Likar-Smiljanic, and T. K. Sarkar, "Wideband frequency-domain characterization of FR-4 and time-domain causality," *IEEE Trans. Electromagn. Compat.*, vol. 43, no. 4, pp. 662–667, Nov. 2001.

[59] S. Sahin, N. K. Nahar, and K. Sertel, "Dielectric properties of low-loss polymers for mmW and THz applications," *J. Infr., Millim., Terahertz Waves*, vol. 40, pp. 557–573, Mar. 2019.

Andrea Alimenti (Member, IEEE) received the B.Sc., M.Sc., and Ph.D. degrees (cum laude) in electronic engineering from University Roma Tre, Rome, Italy, in 2014, 2017, and 2021, respectively.

He is currently a Research Fellow in electrical and electronic measurements with the Department of Industrial, Electronic and Mechanical Engineering (DIIEM), University Roma Tre. His research activities include the development of microwave measurement techniques and methods for the characterization and study of the surface impedance, at cryogenic temperatures and in high magnetic fields, of technological superconductors, the design of microwave resonant fixtures for the characterization of dielectrics, and conducting materials at room temperatures, and the analysis of their metrological characteristics.

Erika Pittella (Member, IEEE) received the M.Sc. (cum laude) and Ph.D. degrees in electronic engineering from the Sapienza University of Rome, Rome, Italy, in 2006 and 2011, respectively.

She is currently an Assistant Professor with the Department of Information Engineering, Electronics and Telecommunications (DIET), Sapienza University of Rome. Her research interests are related to the measurement of complex permittivity of materials, time-domain reflectometry applications, and biomedical instrumentation design. Her research interests also include the modeling of ultrawideband radars for the remote monitoring of cardiorespiratory activity and the design of sources, antennas, and receivers of such systems.

Dr. Pittella is a member of the Working Group "IEEE-SA Standards Project in the Wearable Cuffless Blood Pressure Monitors Working Group," the IEEE Instrumentation and Measurement Society, the IEEE Women in Engineering Affinity Group (Italy Section), and the Italian Group of Electrical and Electronic Measurements (GMEE).

Kostiantyn Torokhtii (Member, IEEE) received the M.S. degree (cum laude) in cryogenic technique and technology from the National Technical University "Kharkiv Polytechnic Institute," Kharkiv, Ukraine, in 2007, and the Ph.D. degree in biomedical electronics, electromagnetism and telecommunication from University Roma Tre, Rome, Italy, in 2013.

From 2013 to 2018, he was a Research Fellow with the Engineering Department, University Roma Tre, where he is currently a Technical Researcher. His current research activities include the design, realization, and application of dielectric resonator-based measurement cells for conductors' surface impedance and dielectrics permittivity measurements in high magnetic fields from room to cryogenic temperatures.

Nicola Pompeo (Senior Member, IEEE) received the M.Sc. degree (Hons.) in electronics engineering from the Sapienza University of Rome, Rome, Italy, in 1998, and the Ph.D. degree in physics from the University Roma Tre, Rome, in 2006.

He is currently an Associate Professor at the Department of Industrial, Electronic and Mechanical Engineering, University Roma Tre. His research activity has been mainly focused on the study and characterization of superconducting materials through surface impedance measurements at microwaves and in medium/high magnetic fields. The studies are aimed at increasing the knowledge of dissipation mechanisms (vortex motion, flux flow, pinning, and creep) as well as at guiding the material optimization (e.g., increased pinning by artificial defects) for applications (e.g., coated conductors for magnets, current transport, beam screens for particle accelerators, microwave resonant detectors for dark matter). He has authored over 100 articles in international journals and conference proceedings. His research interests include the development of systems and techniques for the measurement of superconductor surface impedance as well as the dielectric's complex permittivity, ranging from resonant (dielectric resonators) to wideband (Corbino disk) setups.

Emanuele Piuzzi (Member, IEEE) received the M.S. (cum laude) and Ph.D. degrees in electronic engineering from the Sapienza University of Rome, Rome, Italy, in 1997 and 2001, respectively.

He is currently an Associate Professor in electrical and electronic measurements with the Department of Information Engineering, Electronics and Telecommunications (DIET), Sapienza University of Rome. His current research activities include the measurement of complex permittivity of materials and their application to material characterization and monitoring, biomedical instrumentation design, and evaluation of human exposure to electromagnetic fields.

Dr. Piuzzi is a member of the Italian Group of Electrical and Electronic Measurements (GMEE) and the Italian Electrotechnical Committee (CEI).

Enrico Silva (Senior Member, IEEE) received the M.Sc. degree in physics and the Ph.D. degree in applied electromagnetism from University "La Sapienza," Rome, Italy, in 1990 and 1994, respectively.

He joined as an Assistant Professor in condensed matter physics with the Universitá Roma Tre, Rome, in 1994, where he became an Associate Professor of experimental physics, in 2001. He is a Full Professor in electrical and electronic measurements at the Department of Industrial, Electronic and Mechanical Engineering, University Roma Tre. He has authored over 190 articles in international journals and conference proceedings. His research interests include systems for microwave measurements on conducting materials, special measuring systems operating in cryogenic environments, the measurement of electromagnetic properties of superconductors for practical applications, the measurement of the surface impedance of layered conductors, and the physics of nanostructured superconductors.

Dr. Silva is currently the Chair of the Italian Chapter of the IEEE Council on Superconductivity.